

**Eigenstate entanglement entropy in a  $\mathcal{PT}$ -invariant non-Hermitian system**

Ranjan Modak and Bhabani Prasad Mandal

*Department of Physics, Banaras Hindu University, Varanasi 221005, India* (Received 2 April 2021; accepted 10 June 2021; published 24 June 2021)

Much has been learned about universal properties of the eigenstate entanglement entropy for one-dimensional lattice models, which is described by a Hermitian Hamiltonian, while much less has been understood for non-Hermitian systems. In the present work we study a non-Hermitian, noninteracting model of fermions which is invariant under combined  $PT$  transformation. Our models show a phase transition from a  $PT$  unbroken phase to broken phase as we tune the Hermiticity-breaking parameter. Entanglement entropy of such systems can be defined in two different ways, depending on whether we consider only right (or equivalently, only left) eigenstates or a combination of both left and right eigenstates which form a complete set of biorthonormal eigenstates. We demonstrate that the entanglement entropy of the ground state and also of the typical excited states shows some unique features in both of these phases of the system. Most strikingly, entanglement entropy obtained taking a combination of both left and right eigenstates shows an exponential divergence with system size at the transition point. While in the  $PT$ -unbroken phase, the entanglement entropy obtained from only the right (or equivalently, left) eigenstates shows identical behavior to an equivalent Hermitian system which is connected to the non-Hermitian system by a similarity transformation.

DOI: [10.1103/PhysRevA.103.062416](https://doi.org/10.1103/PhysRevA.103.062416)**I. INTRODUCTION**

Entanglement is a property of quantum systems, providing unique ways of characterizing quantum many-body systems [1,2]. The correlations between two entangled quantum systems that are in an overall pure state cannot be explained by local classical theory [3]. Studies of entanglement indicators have given insights into the properties of ground states [4,5], quantum phase transitions [6,7], and highly excited eigenstates that exhibit eigenstate thermalization [8–11]. Different measures of entanglement have also been given lots of attention in the context of black hole physics [12,13], holography [14,15], and quantum information scrambling in nonequilibrium quantum dynamics [16–18]. Recently, thanks to the advancements of ultracold atoms in an optical lattice, the measurements of an entanglement have been realized even in experiments [19,20].

On the other hand, in recent days the study of non-Hermitian systems, such as open systems or dissipative systems with gain and loss [21–25], has revealed various intriguing phenomena that do not exist in Hermitian systems. For example, the complex energy spectra of non-Hermitian systems are theoretically predicted to host bulk Fermi arcs [26–30], which has been also realized in experiments [31]. Also, there is a growing interest to extend the idea of topological Bloch theory developed in Hermitian systems to non-Hermitian Hamiltonians [32–36].

Among a large class of non-Hermitian systems, if a system is invariant under combined parity and time-reversal ( $PT$ ) operations, they can have purely real spectra for a finite range of parameters [37,38]. The Hermiticity property which is sufficient to ensure the real spectrum of the Hamiltonian in

usual quantum mechanics is replaced by  $PT$  symmetry in the case of non-Hermitian systems. Although the spectrum of such systems may be completely real, the eigenstates may not form an orthonormal set and may not have positive-definite norms. Because of these the probabilistic interpretation of quantum theories fails and the time evolution of the corresponding quantum systems becomes nonunitary. Later a consistent quantum theory with a complete real spectrum, unitary time evolution, and probabilistic interpretation for  $PT$ -symmetric non-Hermitian systems has been developed in a modified Hilbert space equipped with a positive-definite  $CPT$  inner product [39].  $C$  is an additional symmetry associated with every  $PT$ -symmetric non-Hermitian system. Because of this exciting realization, the research in non-Hermitian systems has received a huge boost over the past two decades [40].  $PT$ -symmetric non-Hermitian systems have found numerous applications in various branches of physics and interdisciplinary areas [41–52], and some of the predictions of non-Hermitian theories are experimentally observed [53–56]. Another important aspect is that such  $PT$ -symmetric non-Hermitian systems generally exhibit a phase transition (or, more appropriately, a  $PT$  breaking transition) that separates two parametric regions, (i) a region of the unbroken  $PT$  symmetry in which the entire spectrum is real and eigenstates of the system respect  $PT$  symmetry, and (ii) a region of broken  $PT$  symmetry in which the whole spectrum (or a part of it) appears as complex-conjugate pairs and eigenstates of the Hamiltonian do not respect  $PT$  symmetry [57–63].

One of the most popular examples of  $PT$ -symmetric systems are open systems with balanced gain and loss [64–68]. Typically, in such a system the parity denotes a reflection symmetry in its spatial arrangement, and when balanced gain

and loss leads to non-Hermiticity. Usually for small gain and loss rates, the eigenvalues of the  $PT$ -symmetric Hamiltonian describing such a system remain real; however, when the strength of the gain (or loss) exceeds a value known as the  $PT$ -symmetry-breaking threshold, two or more of its eigenvalues become degenerate and then complex-conjugate pairs. This emergence of complex-conjugate eigenvalues is a signature of  $PT$  symmetry breaking. Recent developments in the fabrication techniques of optical devices can allow one to create and control arrays of coupled optical waveguides, and the couplings of these arrays can be tuned to match the dynamics of a large variety of different tight-binding Hamiltonians [69,70]. Also, controlled loss and gain can be implemented relatively straightforwardly, allowing the observable dynamics to extend into the non-Hermitian realm [54,55].

In this work, our main aim is to understand entanglement properties of the eigenstate of non-Hermitian  $PT$ -symmetric systems. In general, quantum correlation is an extremely useful tool to detect different phases as well as the phase transition. Specially, for one-dimensional (1D) systems on lattice, the scaling of entanglement entropy with system size gives lots of insights regarding the system. In order to distinguish between gapless and gapped phases of a system [71] or detect localization-delocalization transitions [72], the eigenstate entanglement entropy is one of the most popular diagnostics. Here we show that the entanglement entropy also can be used as a probe to detect different phases of  $PT$ -invariant systems as well as  $PT$  transitions. Since the non-Hermitian systems have two types of eigenvectors (left and right), we define the entanglement entropy in two different ways [73], depending on whether we consider only right (or equivalently, only left) eigenstates or a combination of both left and right eigenstates. We find that the entanglement entropy obtained taking a combination of both left and right eigenstates diverges exponentially with system size at the transition point. While in the  $PT$ -unbroken phase, the entanglement entropy obtained from only the right (or equivalently, left) eigenstate shows identical behavior to a Hermitian system.

The paper is organized as follows: In Sec. II we introduce the non-Hermitian lattice model, which is invariant under  $PT$  transformation. Next we discuss our analytical understanding for the  $2 \times 2$  model in Sec. III. In Sec. IV we numerically investigate the  $PT$  transition point, and Sec. V is devoted to the analysis of entanglement entropy of the ground state as well as a typical excited state. Finally, in Sec. VI we summarize our results.

## II. MODEL

We study noninteracting fermions in a 1D lattice with an open boundary. The system is described by the following Hamiltonian:

$$H_0 = - \sum_{j=1}^{L-1} (\hat{c}_j^\dagger \hat{c}_{j+1} + \text{H.c.}), \quad (1)$$

where  $\hat{c}_j^\dagger$  ( $\hat{c}_j$ ) is the fermionic creation (annihilation) operator at site  $j$ , which satisfies standard anticommutation relations.  $L$  is the size of the system, which we set to be an even

number for all our calculations (we choose the lattice spacing as unity).

In order to make the Hamiltonian  $PT$  symmetric and non-Hermitian, we add a local term at site  $L/2$  and  $L/2 + 1$ . The  $PT$ -symmetric Hamiltonian reads

$$H = H_0 + i\gamma(\hat{n}_{L/2} - \hat{n}_{L/2+1}), \quad (2)$$

where  $\hat{n}_j = \hat{c}_j^\dagger \hat{c}_j$  is the number operator, and  $\gamma$  is identified as the Hermiticity-breaking parameter. While under parity transformation  $c_j \rightarrow c_{L-j+1}$ , time-reversal symmetry operation changes  $i \rightarrow -i$ . Hence,  $H$  remains invariant under  $PT$  transformation, which implies  $[H, PT] = 0$ .

For nonzero values of  $\gamma$ ,  $H$  is non-Hermitian. Hence its left eigenvectors  $|L_n\rangle$  and  $R_n\rangle$  are not the same. However,  $H$  is diagonalizable, and  $H = \sum_n \epsilon_n |R_n\rangle \langle L_n|$ , with  $\langle L_n | R_m \rangle = \delta_{mn}$  and  $\langle R_n | R_n \rangle = 1$ .  $\epsilon_n$  can be identified as single-particle energy eigenvalues of the system, which in general is complex. If the Hamiltonian  $H$  goes through a  $PT$  phase transition, then in the  $PT$ -symmetric phase, the  $\epsilon_n$  values remain real. On the other hand, in the broken  $PT$  phase,  $\epsilon_n$  values are complex. We also verified our results for another model where we added the Hermiticity-breaking terms in a  $PT$ -invariant way in four sites, i.e., described by following Hamiltonian:

$$\tilde{H} = H_0 + i\gamma \sum_{j=L/2-(r-1)}^{L/2+r} (-1)^j \hat{n}_j, \quad (3)$$

where we chose  $r = 2$ . We would also like to point out that in the absence of a Hermiticity-breaking term, our model is the same as a nearest-neighbor fermionic ‘‘tight-binding’’ model, which is possibly the simplest exactly solvable model one can write down in the context of condensed-matter physics. Also, we believe that a variant of our Hamiltonian with gain and loss is experimentally realizable in an ultracold fermionic system [74]. Note that for all the many-body calculations, we chose to work at half-filling.

## III. ANALYTICAL RESULTS: $2 \times 2$ MATRIX EXAMPLE

In this section we restrict the Hamiltonian  $H$  to a lattice of only two sites. Our aim is to analytically solve the  $2 \times 2$  matrix to gather some insights about this model. The Hamiltonian  $H$  (2) is represented in matrix form as

$$H^{2 \times 2} = \begin{pmatrix} i\gamma & -1 \\ -1 & -i\gamma \end{pmatrix}. \quad (4)$$

There exist various representations of the parity operator, and we define the parity operator for this model as

$$P = \begin{pmatrix} 0 & 1 \\ 1 & 0 \end{pmatrix}, \quad (5)$$

since  $P$  transforms  $\begin{pmatrix} 1 \\ 0 \end{pmatrix}$  to  $\begin{pmatrix} 0 \\ 1 \end{pmatrix}$  and vice versa. It is an optimal choice for our case. It is straightforward to check that the Hamiltonian in Eq. (4) is  $PT$  invariant. In the first step, we evaluate the eigenvalue of this  $2 \times 2$  matrix, which is

$$E_{\pm} = \pm \sqrt{(1 - \gamma^2)}. \quad (6)$$

It implies that for  $\gamma > 1$  ( $\gamma < 1$ ),  $E_{\pm}$  is completely complex (real). Also, it is straightforward to check that for  $\gamma < 1$ ,

$|E_+\rangle = \frac{1}{\sqrt{2\cos\alpha}} \begin{pmatrix} e^{i\alpha/2} \\ e^{-i\alpha/2} \end{pmatrix}$  and  $|E_-\rangle = \frac{i}{\sqrt{2\cos\alpha}} \begin{pmatrix} e^{-i\alpha/2} \\ -e^{i\alpha/2} \end{pmatrix}$  are simultaneous eigenstates of  $H^{2\times 2}$  [75] and  $PT$ , where  $\sin\alpha = -\gamma$ . Hence, one can conclude that the  $PT$  transition occurs for the  $H^{2\times 2}$  matrix model at  $\gamma = 1$ , and the  $PT$ -symmetric phase corresponds to  $\gamma < 1$ . In the  $PT$  broken phase, for  $\gamma > 1$ ,  $\alpha$  becomes complex and hence the eigenstates  $|E_+\rangle$  and  $|E_-\rangle$  are not eigenstates of  $PT$ .

Now we go one step ahead and construct a new linear operator  $C$  that commutes with both  $H^{2\times 2}$  and  $PT$ . The operator  $C$  for the  $H^{2\times 2}$  matrix turns out to be [40,76]

$$C = \frac{1}{\sqrt{1-\gamma^2}} \begin{pmatrix} -i\gamma & 1 \\ 1 & i\gamma \end{pmatrix}. \quad (7)$$

A more general way to represent the  $C$  operator is to express it generically,  $C = e^{Q/2}P$ . It has been shown that the square root of the positive operator  $e^Q$  can be used to construct a similarity transformation that maps a non-Hermitian  $PT$ -symmetric Hamiltonian  $H$  to an equivalent Hermitian Hamiltonian  $h$  [63], where

$$h = e^{-Q/2} H e^{Q/2}. \quad (8)$$

For the  $H^{2\times 2}$  matrix model, the equivalent Hermitian matrix  $h^{2\times 2}$  will be

$$h^{2\times 2} = \begin{pmatrix} 0 & -\sqrt{1-\gamma^2} \\ -\sqrt{1-\gamma^2} & 0 \end{pmatrix}. \quad (9)$$

Note that  $h^{2\times 2}$  is equivalent to  $H^{2\times 2}$  because it has the same eigenvalues as  $H^{2\times 2}$ . However, the eigenvectors of  $H^{2\times 2}$  and  $h^{2\times 2}$  are not the same but are related to each other with a similarity transformation (see Appendix B for a detailed derivation of the equivalent Hermitian matrix  $h^{4\times 4}$  for the  $4 \times 4$  non-Hermitian Hamiltonian).

#### IV. $PT$ TRANSITION

In this section we investigate the fate of the  $PT$  transition for Hamiltonian Eqs. (2) and (3) in the thermodynamic limit. In the previous section we had shown analytically for the two-sites version of the Hamiltonian Eq. (2), the  $PT$  transition occurs at  $\gamma = 1$ . Here we numerically diagonalize the Hamiltonian  $H$  and  $\tilde{H}$  for different values of  $L$  to obtain all the energy eigenvalues. In order to characterize  $PT$  transition, we plot the fraction of complex eigenvalues  $I$  as a function of  $\gamma$ . We expect that in the  $PT$ -symmetric (unbroken) phase the ratio should be zero, whereas in the  $PT$  broken phase the value of  $I$  should be nonzero. Figure 1 (main panel) shows the variation of  $I$  as a function of  $\gamma$  for different values of  $L$  for the Hamiltonian  $H$ . We see  $I$  jumps from 0 to 1 (which implies that all eigenvalues become complex in the  $PT$  broken phase) at  $\gamma = 1$ , which concludes a clear signature  $PT$  phase transition in this model, where the  $PT$  broken (unbroken) phase corresponds to  $\gamma > 1$  ( $\gamma < 1$ ). Interestingly, this transition point  $\gamma_{th} = 1$  obtained from our numerical results is exactly the same as what we obtained by analyzing the  $2 \times 2$  matrix in the previous section.

We would also like to point out that the  $PT$  transition we observed for Hamiltonian Eq. (2) is unique in the sense that here in the  $PT$  broken phase all energy eigenvalues are

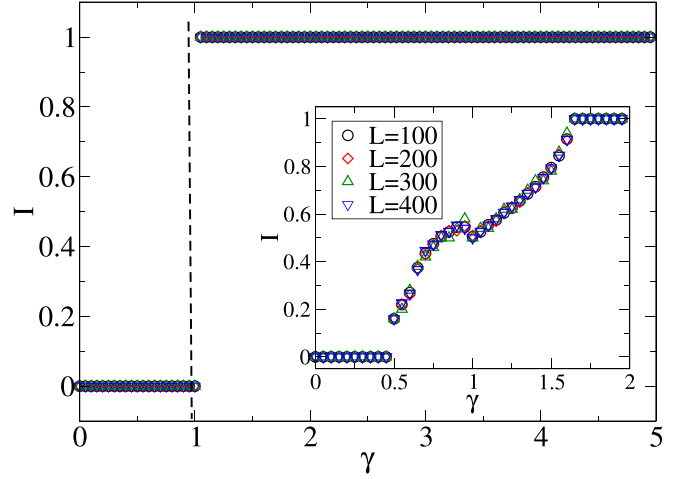


FIG. 1. Variation of the fraction of single-particle complex eigenvalues  $I$  as a function of the Hermiticity-breaking parameter  $\gamma$  for  $L = 100, 200, 300,$  and  $400$  for the Hamiltonian  $H$  (2). Inset shows the variation of the fraction of single-particle complex eigenvalues  $I$  as a function  $\gamma$ , where the Hermiticity-breaking terms have been added in four sites [see Hamiltonian  $\tilde{H}$  (3)].

complex, and hence at  $\gamma = 1$ , the fraction of complex eigenvalues  $I$  jumps from 0 to 1. However, this feature is just a manifestation of the fact that we have added the Hermiticity-breaking parameter only at sites  $L/2$  and  $L/2 + 1$ . In the inset of Fig. 1, we have studied the Hamiltonian  $\tilde{H}$  [see Eq. (3)] where we have added the Hermiticity-breaking terms in four sites. We show that the  $PT$  transition points  $\gamma_{th} \simeq 0.45 < 1$ , and also we find that here  $I$  does not jump sharply from 0 to 1; in contrast, there is a parameter regime where  $I$  takes values between  $[0,1]$ . This implies that in that parameter regime, a fraction of eigenvalues still remains real. However, as we increase  $\gamma$  all energy eigenvalues become complex. Interestingly, we also note that for this model near  $\gamma = 1$  the variation of  $I$  with  $\gamma$  is nonmonotonic. There is a parameter regime near  $\gamma = 1$  for which the number of complex eigenvalues decreases as we increase the Hermiticity-breaking parameter. Figure 2 shows the variation of  $I$  with  $\gamma$  for the Hamiltonian Eq. (3) for different values of  $r$  and for  $L = 400$ . We find that, indeed,  $\gamma_{th}$  becomes much smaller as we increase  $r$ . The inset shows that  $\gamma_{th}$  approaches zero with  $r$  as a power law. Interestingly, we find that as the number of Hermiticity-breaking terms increases, the region where real and imaginary eigenvalues coexist, i.e.,  $0 < I < 1$ , also increases. Note that it is straightforward to show, even analytically, that the  $PT$ -symmetric phase would not have been stable in the thermodynamic limit if we had added a Hermiticity-breaking term at all sites (see Appendix A for more details).

#### V. ENTANGLEMENT ENTROPY

In this section we will discuss the many-body eigenstate entanglement entropy of the  $PT$ -invariant Hamiltonian (2). We note that a typical measure of the entanglement in a quantum system is bipartite von Neumann entanglement entropy  $S$ , defined as  $S = -\text{Tr}_A[\rho_A \ln \rho_A]$ , where  $\rho_A = \text{Tr}_B \rho$  is the reduced density matrix of a subsystem  $A$  after dividing the

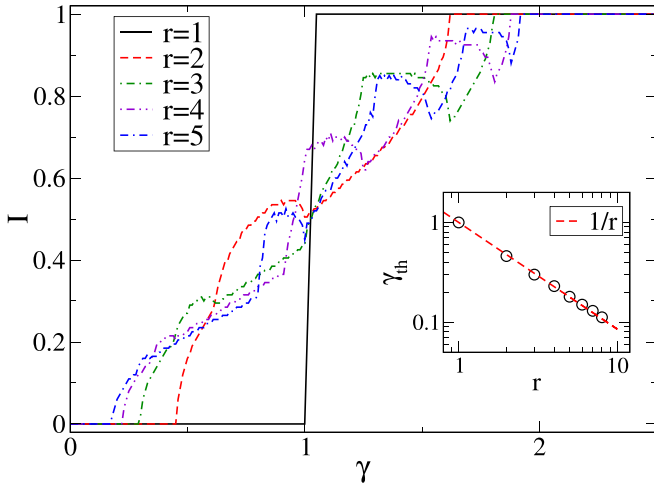


FIG. 2. Variation of the fraction of single-particle complex eigenvalues  $I$  as a function of the Hermiticity-breaking parameter  $\gamma$  for  $L = 400$ , Hamiltonian  $H$  (3) for different values of  $r$ . Inset shows  $\gamma_{th}$  scales to zero with increasing  $r$  as a power law. Dashed line corresponds to  $1/r$ .

system into two adjacent parts  $A$  and  $B$ . and  $\rho$  is the total density matrix corresponding to the eigenstate of the system. For the Hermitian system,  $\rho = |E_n\rangle\langle E_n|$ , where  $E_n$ s are many-body energy eigenstates. For non-Hermitian systems, since left and right eigenvectors are not the same, we have two choices to define the total many-body density matrix of the system, i.e., (1)  $\rho_1 = |R_n\rangle\langle R_n|$  and (2)  $\rho_2 = |L_n\rangle\langle L_n|$ , and the corresponding entanglement entropies are denoted by  $S^R$  and  $S^{LR}$ , respectively [77,78]. Note that since the Hamiltonian Eq. (2) is quadratic, the ground-state (also typical eigenstates) entanglement entropy can be obtained from the one-body density matrix [73] in a similar spirit as one can do for a Hermitian system [79–84].

Also, motivated by our analysis for a two-site model, we conjecture that the Hermitian equivalent model  $h$  corresponds to the non-Hermitian Hamiltonian  $H$  given by

$$h = - \sum_{j=1}^{L/2-1} (\hat{c}_j^\dagger \hat{c}_{j+1} + \text{H.c.}) - \sum_{j=L/2+1}^{L-1} (\hat{c}_j^\dagger \hat{c}_{j+1} + \text{H.c.}) - (1 - \gamma^2)^{1/2} (\hat{c}_{L/2}^\dagger \hat{c}_{L/2+1} + \text{H.c.}). \quad (10)$$

Note that if we restrict ourselves to  $L = 2$ , the Hamiltonian  $h$  becomes identical to  $h^{2 \times 2}$  [see Eq. (9)]. We also test our conjecture by comparing the single-particle energy eigenvalues  $E_n$  for both Hamiltonians (2) and (10) in Fig. 3. We find an excellent agreement between them, as shown in Fig. 3. Next, our goal is to analyze the entanglement entropy of the ground state as well as the typical excited states for both models  $H$  [see Eq. (2)] and  $h$  [see Eq. (10)] and compare their results.

### A. Ground state

We first focus on the ground-state entanglement entropy of the non-Hermitian Hamiltonian  $H$ . Usually the many-body ground state of a noninteracting system is obtained by populating the lowest energy single-particle states one by one. A similar method can also be used for the non-Hermitian system

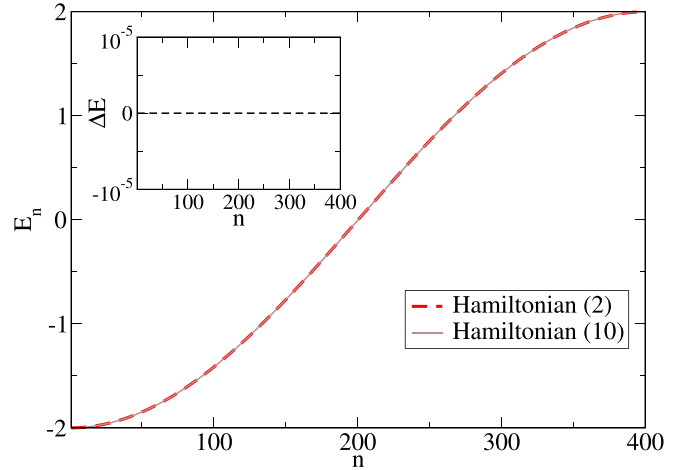


FIG. 3. Comparison of energy eigenvalues  $E_n$  between Hamiltonian (2) and Hamiltonian (10) for  $\gamma = 0.5$  and  $L = 400$ . Inset shows the differences of the energy eigenvalues between Hamiltonian (2) and Hamiltonian (10) are of the order of machine precision.

in the  $PT$ -symmetric phase, given that the energy eigenvalues are purely real. In the case of a  $PT$  broken phase, given that the eigenvalues can be complex, there is a bit of ambiguity regarding in which order we should populate the single-particle states to get the desired many-body ground state. However, we arrange the eigenvalues, sorting by its real parts, and obtain the many-body ground state by populating one by one the single-particle states whose real parts of the eigenvalues are the lowest. Given that we have always restricted ourselves to the even number of particles in the system, this particular choice of the many-body ground state ensures that many-body ground-state energy always remains real, even in the  $PT$  broken phase. Moreover, this working definition of the many-body ground state can also be “analytically continued” in the  $PT$ -symmetric phase.

Figure 4 shows the variation of the ground-state entanglement entropy obtained from the right eigenvectors. In the main panel of Fig. 4, we plot the real part of  $S^R$  as a function of  $\gamma$ . Interestingly, we find that  $S^R$  decreases monotonically as a function of  $\gamma$  when  $\gamma < 1$ , i.e., the  $PT$ -symmetric phase. Remarkably, this value goes to zero at the transition point, i.e.,  $\gamma = 1$ . The solid dashed lines in the main panel of Fig. 4 correspond to the ground-state entanglement entropy of the Hermitian Hamiltonian  $h$ . It shows excellent agreement with the real part of  $S^R$  in the  $PT$ -symmetric phase. In Fig. 4(a), we also plot the variation of the imaginary part of  $S^R$ , we find that while it is zero in the  $PT$ -symmetric phase, for  $\gamma > 1$  (in the broken  $PT$  phase) the imaginary part of  $S^R$  can have nonzero values. We also like to emphasize that  $\text{Re}[S^R]$  vanishes at  $\gamma = 1$  due to the fact that we choose  $L_A = L/2$ . That becomes even more apparent from our Hermitian equivalent Hamiltonian (10). At  $\gamma = 1$ , Hamiltonian (10) is just two separate systems of length  $L/2$  who do not talk to each other. Hence the entanglement entropy is bound to be zero if we make a cut in the middle. However, if we choose  $L_A = L/4$ , at  $\gamma = 1$ , the entanglement will not be zero, shown explicitly in Fig. 4(b). However, the variation of the entanglement

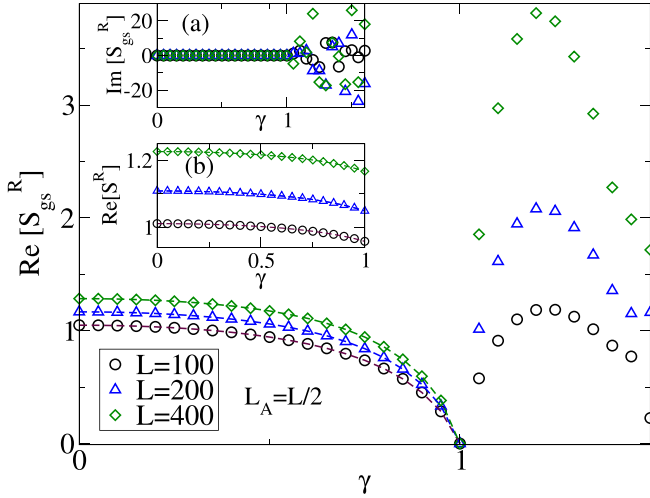


FIG. 4. Variation of the real part of  $S^R$  of the ground state as a function of  $\gamma$  for  $L = 100, 200, 400$ . We choose the subsystem size  $L_A = L/2$ . Solid dashed lines correspond to ground-state entanglement entropy of the Hermitian model  $h$  (10). Inset (a) shows the variation of the imaginary part of  $S^R$  of the ground state as a function of  $\gamma$ . Inset (b) shows the variation of the real part of  $S^R$  of the ground state as a function of  $\gamma$  for subsystem size  $L_A = L/4$ . Solid dashed lines correspond to ground-state entanglement entropy of the Hermitian model  $h$  (10).

entropy in the  $PT$ -symmetric phase can still be captured by the Hermitian equivalent Hamiltonian Eq. (10).

Next we investigate how  $S^{LR}$  behaves as a function of the Hermiticity-breaking parameter  $\gamma$ . We again focus on the ground state. In the main panel of Fig. 5, we plot the

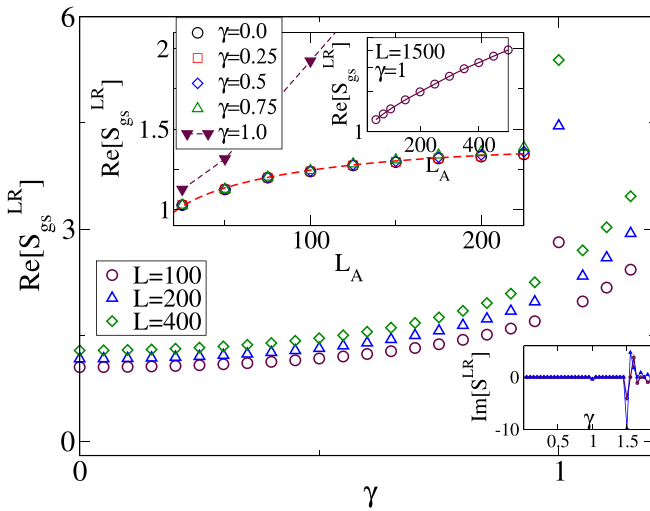


FIG. 5. In the main panel we show the variation of the real part of  $S^{LR}$  of the ground state as a function of  $\gamma$  for  $L = 100, 200, 400$ . We choose the subsystem size  $L_A = L/2$ . Inset shows the variation of the real part of  $S^{LR}$  with  $L_A$  for  $\gamma = 0, 0.25, 0.5, 0.75, 1$ . We keep  $L = 600$  fixed. The red dashed line is the best fit where the fitting function is  $\frac{1}{6} \ln[\sin(\pi L_A/L)] + \text{const}$ . Another inset shows the variation  $\text{Re}[S^{LR}]$  with  $L_A$  (for fixed  $L = 1500$ ) for  $\gamma = 1$  in the semilog scale. Inset in the right-bottom corner shows the variation of the imaginary part of  $S^{LR}$  with  $\gamma$ .

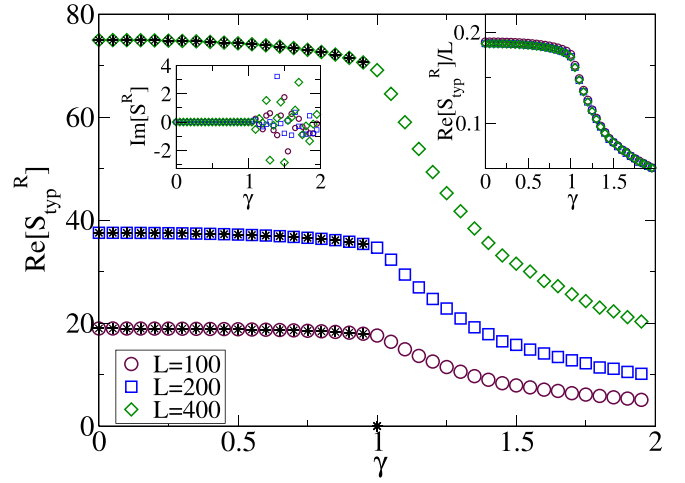


FIG. 6. Variation of  $\text{Re}[S^R]$  of typical eigenstates of the Hamiltonian (2) as a function of  $\gamma$  for  $L = 100, 200, 400$  for fixed  $L_A = L/2$ . Black symbols correspond to the entanglement entropy of a typical state for the Hermitian Hamiltonian  $h$ . Top-right inset shows a nice data collapse when we rescale  $\text{Re}[S^R]$  by  $\text{Re}[S^R]/L_A$ . Another inset shows the variation of imaginary part of  $S^R$  with  $\gamma$ .

real part of  $S^{LR}$  with  $\gamma$  for different values of  $L$ ; we keep the subsystem size  $L_A = L/2$  fixed. We find that in the  $PT$ -symmetric phase and for a fixed value of  $\gamma$ , the real part of  $S^{LR}$  increases with system size. First we focus on the  $PT$ -symmetric phase, i.e.,  $\gamma < 1$ . For  $\gamma = 0$  we know that the Hamiltonian  $H$  is gapless, which implies that the ground state can be described by a conformal field theory (CFT) of central charge  $c$ . Hence we expect that the entanglement entropy  $S$  should scale as  $S = \frac{c}{6} \ln[\sin(\pi L_A/L)] + \text{const}$  [85]. It is well known that the central charge corresponding to the Hamiltonian  $H_0$  is  $c = 1$ . In the inset of Fig. 5, we show that indeed for  $\gamma = 0$ ,  $S$  obeys expected logarithmic scaling. Strikingly, we find that the same scaling exists for  $S^{LR}$  in the  $PT$ -symmetric phase as well. Next we investigate the behavior of  $S^{LR}$  at the phase transition point, i.e.,  $\gamma = 1$ . We observe that at  $\gamma = 1$  the value of  $\text{Re}[S^{LR}]$  is much larger compared to its value in the  $PT$ -symmetric phase. In the inset we show the variation of  $\text{Re}[S^{LR}]$  with  $L_A$  for a fixed value of  $L$ , and we find that  $S^{LR}$  actually diverges exponentially with  $L_A$  at the phase transition point. We also show the variation of the imaginary part of  $S^{LR}$  in the right-bottom corner inset of Fig. 5 and find that in the  $PT$ -symmetric phase the imaginary part of  $S^{LR}$  is zero, whereas in the  $PT$  broken phase it can have nonzero value.

## B. Typical eigenstates

After investigating the ground-state entanglement entropy, now we study the entanglement entropy of the typical states. Again, we investigate separately both  $S^R$  and  $S^{LR}$ . In each configuration, we randomly populate  $L/2$  numbers of particles in total  $L$  number of single-particle states. Then we average over 1000 different configurations [79–81,86]. Figure 6 shows the variation of the real part of  $S^R$  of a typical state with  $\gamma$  for the Hamiltonian  $H$ , Eq. (2). We see that in the  $PT$  unbroken phase, the magnitude of  $S^R$  does not change significantly, it

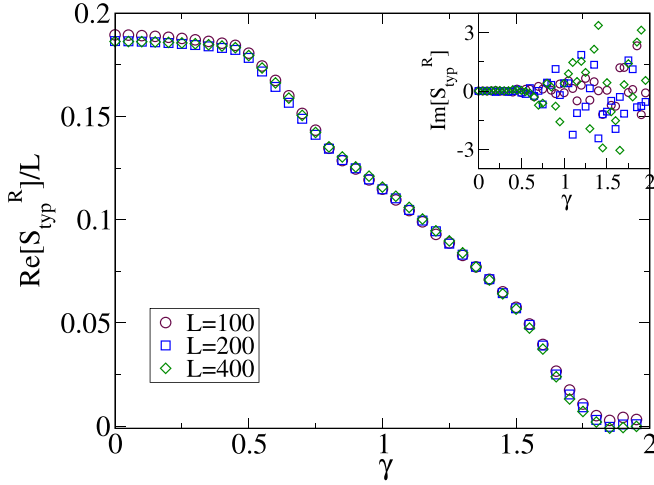


FIG. 7. Variation of  $\text{Re}[S^R]/L$  of typical eigenstates of the Hamiltonian (3) as a function of  $\gamma$  for  $L = 100, 200, 400$  for fixed  $L_A = L/2$ , which shows nice data collapse. Inset shows the variation of  $\text{Im}[S^R]$  with  $\gamma$  for the same model.

remains almost the same as the value obtained for  $\gamma = 0$ . However, for  $\gamma > 1$ , the value monotonically decreases. Also, similar to the ground state,  $\text{Re}[S^R]$  in the  $PT$ -symmetric phase is almost the same as the entanglement obtained for the typical eigenstates of the Hermitian Hamiltonian  $h$  (10). In the inset we show the data collapse when we rescale  $\text{Re}[S^R]$  by  $\text{Re}[S^R]/L_A$ , which indicates the signature of the volume law. We strengthen our claims by investigating the Hamiltonian equation (3) in Fig. 7 as well.

Next we investigate the real part of  $S^{LR}/L$  in Fig. 8 for the Hamiltonian  $\tilde{H}$  (3). We again find a nice data collapse in the  $PT$ -symmetric phase, i.e.,  $\gamma < 0.45$ , which indicates the volume entanglement. However, at the transition point

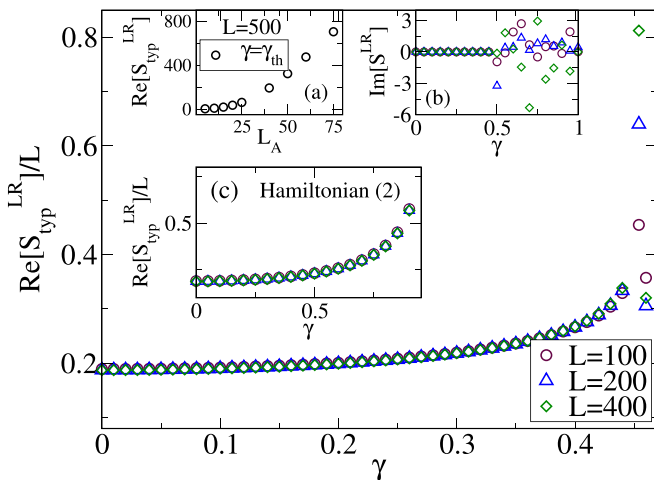


FIG. 8. Variation of  $\text{Re}[S^{LR}]/L$  of typical eigenstates as a function of  $\gamma$  for  $L = 100, 200, 400$  for fixed  $L_A = L/2$  and for the Hamiltonian  $\tilde{H}$  (3). Data collapse is observed for  $\gamma < \gamma_{th} \simeq 0.45$ . Inset (a) shows the variation of  $\text{Re}[S^{LR}_{typ}]$  with  $L_A$  for  $L = 500$  and  $\gamma = \gamma_{th}$ . Inset (b) shows the variation of the imaginary part of  $S^{LR}$  with  $\gamma$ . Inset (c) shows the data collapse of  $S^{LR}/L$  for Hamiltonian Eq. (2) in the  $PT$ -symmetric phase, i.e.,  $\gamma < 1$ .

$\gamma \simeq 0.45$ , the volume-law scaling breaks down. At the point of the phase transition, even after we rescale  $\text{Re}[S^{LR}]$  by  $\text{Re}[S^{LR}]/L$ , the value increases with  $L$ , which suggests the scaling is much faster than the volume law. In Fig. 8(a) we plot the variation  $\text{Re}[S^{LR}]$  for the Hamiltonian  $\tilde{H}$  at the  $PT$  transition point with  $L_A$  for a fixed  $L = 500$ , and we confirm that the scaling of  $\text{Re}[S^{LR}]$  with system size is much faster than the volume-law scaling observed in the  $PT$ -symmetric phase. We also show the imaginary part of  $S^{LR}$  for a typical state in inset (b), which shows that similar to our previous findings in the  $PT$ -symmetric (broken) phase  $\text{Im}[S^{LR}]$  is zero (nonzero). Note that a similar behavior has been observed even for the Hamiltonian  $H$  (2). In Fig. 8(c) we show a nice data collapse for  $S^{LR}/L$  in  $PT$ -symmetric phase, i.e.,  $\gamma < 1$ .

## VI. CONCLUSIONS

In this paper we investigate the entanglement properties of the ground state and a typical excited state of a noninteracting non-Hermitian lattice model which is invariant under  $PT$  transformation. The model we had looked into has two parts. The Hermitian part is described by a fermionic system having just nearest-neighbor hopping, while we add the Hermiticity-breaking terms (also known as gain-loss terms) only at the two sites (four sites for the Hamiltonian  $\tilde{H}$ ), which are situated in the middle of the lattice. Usually in a Hermitian system, if one adds some local perturbations it does not significantly alter the extensive quantities such as energy of the system. Strikingly, here we find that even though we have added the Hermiticity-breaking terms only in a finite number of sites [in two sites for Hamiltonian (2) and in four sites for Hamiltonian (3)], but it significantly modifies the properties of the system. Most importantly, we find that the non-Hermitian model shows a  $PT$  phase transition as we change the Hermiticity-breaking parameter.

Next we analyze the entanglement properties of different phases of this model. We find that in the  $PT$ -symmetric phase, the entanglement entropy obtained from only the right eigenvectors are the same as the entanglement entropy obtained for the equivalent Hermitian model. We find this result extremely nontrivial, given that the equivalence between the non-Hermitian and Hermitian model implies they have the same set of energy eigenvalues, but it does not imply that the eigenvectors of these two models are the same. Hence it is not at all obvious that entanglement entropy of the eigenstates of these two models should be the same.

Another interesting finding of our work is that the entanglement entropy obtained by considering both left and right vectors diverges exponentially with system size at the  $PT$  phase transition point. On the other hand, in the  $PT$ -symmetric phase, the ground-state entanglement entropy scales logarithmically with subsystem size, which is an evidence that presumably low energy states of this  $PT$ -symmetric non-Hermitian system might also be described by CFT. We also find that the typical excited states are volume-law entangled. We would also like to point out that we have repeated all our calculations for the models where we have added the Hermiticity-breaking parameters at more than four sites. We find that even though the results change quantitatively, qualitative features of the entanglement entropy remain unaltered.

Interestingly, the  $PT$  phase transition point  $\gamma_{th}$  approaches zero as we increase the number of non-Hermitian sites; hence we only show the results for the Hamiltonian  $H$  (2) and  $\tilde{H}$  (3).

Our future plan is to understand the effect of interaction and disorder in such systems and study how they modify the  $PT$  phase transitions. Recently, there have been efforts to investigate a non-Hermitian many-body localized phase [87], and it will be interesting to investigate the  $PT$ -symmetric system in the same light.

### ACKNOWLEDGMENTS

R.M. acknowledges the support of a DST-Inspire fellowship by the Department of Science and Technology, Government of India. The authors would like to thank Debraj Rakshit for many stimulating discussions.

### APPENDIX A

Here we investigate a similar model as (2), but we add a complex on-site potential in each site [88]. The model is described by the following Hamiltonian:

$$\tilde{H} = H_0 + i\gamma \sum_j (-)^j \hat{n}_j. \quad (\text{A1})$$

It is straightforward to verify that the Hamiltonian (A1) is also invariant under  $PT$  transformation, i.e.,  $[\tilde{H}, PT] = 0$ .

Thus we arrive at the stationary discrete Schrödinger equation,

$$E\psi_j = \psi_{j+1} + \psi_{j-1} + i\gamma(-1)^j \psi_j. \quad (\text{A2})$$

We assume a trial solution  $\psi_j = Ae^{ijk} + Be^{-ijk}$ . Using the boundary condition  $\psi_0 = \psi_{L+1} = 0$ , one obtains  $A = -B$  and  $k = s\pi/(L+1)$ , with  $s = 0, 1, \dots, L-1$ . Inserting the trial solution of Eq. (A2), it is straightforward to obtain the energy

eigenvalues, which is given by

$$E^2 = 4\cos^2 k - \gamma^2. \quad (\text{A3})$$

From Eq. (A3), one gets that all eigenvalues are real for  $\gamma < 2\cos k$  for any value of  $s$ . Since the smallest value of  $\cos k$  occurs for  $s = L/2$ , the condition of a completely real spectrum is

$$\gamma < \gamma_{th} = 2\cos\left[\frac{L\pi}{2(L+1)}\right] \simeq \pi/L. \quad (\text{A4})$$

Hence, in the thermodynamic limit the Hamiltonian (A1) does not have a true  $PT$ -unbroken phase.

### APPENDIX B

In this section we restrict the Hamiltonian  $\tilde{H}$ , Eq. (3), to a lattice of only four sites. We show the details of the numerical calculation, which one can use to obtain the Hermitian equivalent Hamiltonian for this system. The outline of the calculation is already presented in the main text in Sec. III. The Hamiltonian  $4 \times 4$  is represented in the matrix form as

$$H^{4 \times 4} = \begin{pmatrix} i\gamma & -1 & 0 & 0 \\ -1 & -i\gamma & -1 & 0 \\ 0 & -1 & i\gamma & -1 \\ 0 & 0 & -1 & -i\gamma \end{pmatrix}. \quad (\text{B1})$$

We choose  $\gamma = 0.2$ , for which all energy eigenvalues are completely real, i.e.,  $E_1 = -1.60563$ ,  $E_2 = 1.60563$ ,  $E_3 = 0.584779$ , and  $E_4 = -0.584779$ . Hence it belongs to the  $PT$ -symmetric phase. Simultaneous eigenvectors of  $H^{4 \times 4}$  and  $PT$  are  $|E_1\rangle = (0.373182, 0.59919 + 0.07463i, 0.603821, 0.37032 + 0.0461278i)^T$ ,  $|E_2\rangle = (0.373182, -0.59919 + 0.07463i, 0.603821, -0.37032 + 0.0461278i)^T$ ,  $|E_3\rangle = (0.585094 + 0.200108i, -0.382172, -0.361608 - 0.123674i, 0.618368)^T$ , and  $|E_4\rangle = (0.618368, 0.361608 + 0.123674i, -0.382172, -0.585094 - 0.200108i)^T$ , where  $PT|E_{1,3}\rangle = |E_{1,3}\rangle$ , and  $PT|E_{2,4}\rangle = -|E_{2,4}\rangle$ . Now it is straightforward to obtain the  $C$  operator, where  $C^2 = I$ , and  $[C, H^{4 \times 4}] = 0$ , it reads as

$$C = \begin{pmatrix} -0.2819i & 0.92331 & 0.097245i & -0.486228 \\ 0.92331 & 0.184663i & 0.437088 & -0.097245i \\ 0.097245i & 0.437088 & -0.184663i & 0.92331 \\ -0.486228 & -0.097245i & 0.923316 & 0.2819i \end{pmatrix}.$$

Given that  $C = e^Q P$ , the parity operator reads

$$P = \begin{pmatrix} 0 & 0 & 0 & 1 \\ 0 & 0 & 1 & 0 \\ 0 & 1 & 0 & 0 \\ 1 & 0 & 0 & 0 \end{pmatrix}, \quad (\text{B2})$$

and it is trivial to obtain  $h^{4 \times 4} = e^{-Q/2} H^{4 \times 4} e^{Q/2}$ , which is represented as,

$$h^{4 \times 4} = \begin{pmatrix} 0 & -0.979579 & 0 & -0.0206343 \\ -0.979579 & 0 & -1.00021 & 0 \\ 0 & -1.00021 & 0 & -0.979579 \\ -0.0206343 & 0 & -0.979579 & 0 \end{pmatrix},$$

where  $h^{4\times 4}$  is a Hermitian matrix, and it is straightforward to check that its eigenvalues are same as the eigenvalues of  $H^{4\times 4}$ , i.e.,  $E_1, E_2, E_3$ , and  $E_4$ . Note that one can perform a similar calculation for any  $PT$ -symmetric non-Hermitian system and obtain the Hermitian equivalent Hamiltonian.

- 
- [1] J. Eisert, M. Cramer, and M. B. Plenio, *Rev. Mod. Phys.* **82**, 277 (2010).
- [2] L. Amico, R. Fazio, A. Osterloh, and V. Vedral, *Rev. Mod. Phys.* **80**, 517 (2008).
- [3] A. Einstein, B. Podolsky, and N. Rosen, *Phys. Rev.* **47**, 777 (1935).
- [4] G. Vidal, J. I. Latorre, E. Rico, and A. Kitaev, *Phys. Rev. Lett.* **90**, 227902 (2003).
- [5] K. Audenaert, J. Eisert, M. B. Plenio, and R. F. Werner, *Phys. Rev. A* **66**, 042327 (2002).
- [6] T. J. Osborne and M. A. Nielsen, *Phys. Rev. A* **66**, 032110 (2002).
- [7] A. Osterloh, L. Amico, G. Falci, and R. Fazio, *Nature (London)* **416**, 608 (2002).
- [8] J. M. Deutsch, *Phys. Rev. A* **43**, 2046 (1991).
- [9] M. Rigol, V. Dunjko, and M. Olshanii, *Nature (London)* **452**, 854 (2008).
- [10] M. Srednicki, *Phys. Rev. E* **50**, 888 (1994).
- [11] L. D'Alessio, Y. Kafri, A. Polkovnikov, and M. Rigol, *Adv. Phys.* **65**, 239 (2016).
- [12] M. Srednicki, *Phys. Rev. Lett.* **71**, 666 (1993).
- [13] L. Bombelli, R. K. Koul, J. Lee, and R. D. Sorkin, *Phys. Rev. D* **34**, 373 (1986).
- [14] S. Ryu and T. Takayanagi, *Phys. Rev. Lett.* **96**, 181602 (2006).
- [15] A. Lewkowycz and J. Maldacena, *J. High Energy Phys.* **08** (2013) 090.
- [16] R. Lewis-Swan, A. Safavi-Naini, J. J. Bollinger, and A. M. Rey, *Nat. Commun.* **10**, 1 (2019).
- [17] V. Alba and P. Calabrese, *Phys. Rev. B* **100**, 115150 (2019).
- [18] R. Modak, V. Alba, and P. Calabrese, *J. Stat. Mech.: Theory Exp.* (2020) 083110.
- [19] R. Islam, R. Ma, P. M. Preiss, M. E. Tai, A. Lukin, M. Rispoli, and M. Greiner, *Nature (London)* **528**, 77 (2015).
- [20] A. M. Kaufman, M. E. Tai, A. Lukin, M. Rispoli, R. Schittko, P. M. Preiss, and M. Greiner, *Science* **353**, 794 (2016).
- [21] H. Xu, D. Mason, L. Jiang, and J. Harris, *Nature (London)* **537**, 80 (2016).
- [22] H. J. Carmichael, *Phys. Rev. Lett.* **70**, 2273 (1993).
- [23] J. Y. Lee, J. Ahn, H. Zhou, and A. Vishwanath, *Phys. Rev. Lett.* **123**, 206404 (2019).
- [24] V. V. Konotop, J. Yang, and D. A. Zezyulin, *Rev. Mod. Phys.* **88**, 035002 (2016).
- [25] K. Kawabata, Y. Ashida, and M. Ueda, *Phys. Rev. Lett.* **119**, 190401 (2017).
- [26] K. Moors, A. A. Zyuzin, A. Y. Zyuzin, R. P. Tiwari, and T. L. Schmidt, *Phys. Rev. B* **99**, 041116(R) (2019).
- [27] J. Carlström and E. J. Bergholtz, *Phys. Rev. A* **98**, 042114 (2018).
- [28] J. C. Budich, J. Carlström, F. K. Kunst, and E. J. Bergholtz, *Phys. Rev. B* **99**, 041406(R) (2019).
- [29] Z. Yang and J. Hu, *Phys. Rev. B* **99**, 081102(R) (2019).
- [30] T. Yoshida, R. Peters, N. Kawakami, and Y. Hatsugai, *Phys. Rev. B* **99**, 121101(R) (2019).
- [31] K. Ding, G. Ma, Z. Q. Zhang, and C. T. Chan, *Phys. Rev. Lett.* **121**, 085702 (2018).
- [32] F. Song, S. Yao, and Z. Wang, *Phys. Rev. Lett.* **123**, 246801 (2019).
- [33] S. Yao, F. Song, and Z. Wang, *Phys. Rev. Lett.* **121**, 136802 (2018).
- [34] K.-I. Imura and Y. Takane, *Phys. Rev. B* **100**, 165430 (2019).
- [35] C. H. Lee, L. Li, and J. Gong, *Phys. Rev. Lett.* **123**, 016805 (2019).
- [36] C. H. Lee, G. Li, Y. Liu, T. Tai, R. Thomale, and X. Zhang, *arXiv:1812.02011*.
- [37] C. M. Bender, D. C. Brody, and H. F. Jones, *Phys. Rev. Lett.* **89**, 270401 (2002).
- [38] C. M. Bender and S. Boettcher, *Phys. Rev. Lett.* **80**, 5243 (1998).
- [39] Consistent quantum theories with a bigger class of non-Hermitian systems described by pseudo-Hermitian Hamiltonians have also been formulated in a similar fashion [40,89].
- [40] C. M. Bender, *Rep. Prog. Phys.* **70**, 947 (2007).
- [41] B. P. Mandal and A. Ghatak, *J. Phys. A: Math. Theor.* **45**, 444022 (2012).
- [42] A. Mostafazadeh, *Phys. Rev. Lett.* **102**, 220402 (2009).
- [43] A. Ghatak, M. Hasan, and B. P. Mandal, *Phys. Lett. A* **379**, 1326 (2015).
- [44] M. Hasan and B. P. Mandal, *Eur. Phys. J. Plus* **135**, 1 (2020).
- [45] M. V. Berry, *Czech. J. Phys.* **54**, 1039 (2004).
- [46] W. Heiss, *Phys. Rep.* **242**, 443 (1994).
- [47] C. F. Gmachl, *Nature (London)* **467**, 37 (2010).
- [48] W. Wan, Y. Chong, L. Ge, H. Noh, A. D. Stone, and H. Cao, *Science* **331**, 889 (2011).
- [49] N. Liu, M. Mesch, T. Weiss, M. Hentschel, and H. Giessen, *Nano Lett.* **10**, 2342 (2010).
- [50] A. Mostafazadeh and M. Sarisaman, *Proc. R. Soc. A* **468**, 3224 (2012).
- [51] M. Hasan and B. P. Mandal, *Ann. Phys.* **396**, 371 (2018).
- [52] M. Hasan and B. P. Mandal, *Ann. Phys.* **391**, 240 (2018).
- [53] Z. H. Musslimani, K. G. Makris, R. El-Ganainy, and D. N. Christodoulides, *Phys. Rev. Lett.* **100**, 030402 (2008).
- [54] C. E. Rüter, K. G. Makris, R. El-Ganainy, D. N. Christodoulides, M. Segev, and D. Kip, *Nat. Phys.* **6**, 192 (2010).
- [55] R. El-Ganainy, K. Makris, D. Christodoulides, and Z. H. Musslimani, *Opt. Lett.* **32**, 2632 (2007).
- [56] A. Guo, G. J. Salamo, D. Duchesne, R. Morandotti, M. Volatier-Ravat, V. Aimez, G. A. Siviloglou, and D. N. Christodoulides, *Phys. Rev. Lett.* **103**, 093902 (2009).
- [57] M. Znojil, *J. Phys. A: Math. Gen.* **36**, 7825 (2003).
- [58] B. P. Mandal, B. K. Mourya, K. Ali, and A. Ghatak, *Ann. Phys.* **363**, 185 (2015).
- [59] C. M. Bender, S. Boettcher, and P. N. Meisinger, *J. Math. Phys.* **40**, 2201 (1999).

- [60] B. P. Mandal, *Mod. Phys. Lett. A* **20**, 655 (2005).
- [61] C. T. West, T. Kottos, and T. Prosen, *Phys. Rev. Lett.* **104**, 054102 (2010).
- [62] A. Nanayakkara, *Phys. Lett. A* **304**, 67 (2002).
- [63] C. M. Bender, G. V. Dunne, P. N. Meisinger, and M. Şimşek, *Phys. Lett. A* **281**, 311 (2001).
- [64] E. Lee, H. Lee, and B.-J. Yang, *Phys. Rev. B* **101**, 121109(R) (2020).
- [65] A. Khare and B. P. Mandal, *Phys. Lett. A* **272**, 53 (2000).
- [66] B. P. Mandal, B. K. Mourya, and R. K. Yadav, *Phys. Lett. A* **377**, 1043 (2013).
- [67] H. Raval and B. P. Mandal, *Nucl. Phys. B* **946**, 114699 (2019).
- [68] Y. Liu, Y. Wang, X.-J. Liu, Q. Zhou, and S. Chen, *Phys. Rev. B* **103**, 014203 (2021).
- [69] U. Peschel, T. Pertsch, and F. Lederer, *Opt. Lett.* **23**, 1701 (1998).
- [70] D. N. Christodoulides, F. Lederer, and Y. Silberberg, *Nature (London)* **424**, 817 (2003).
- [71] A. Biswas, R. Prabhu, A. Sen(De), and U. Sen, *Phys. Rev. A* **90**, 032301 (2014).
- [72] D. A. Abanin, E. Altman, I. Bloch, and M. Serbyn, *Rev. Mod. Phys.* **91**, 021001 (2019).
- [73] L. Herviou, N. Regnault, and J. H. Bardarson, *SciPost Phys.* **7**, 069 (2019).
- [74] K. Yokomizo and S. Murakami, *Phys. Rev. Lett.* **123**, 066404 (2019).
- [75] C. M. Bender, J. Brod, A. Refig, and M. E. Reuter, *J. Phys. A: Math. Gen.* **37**, 10139 (2004).
- [76] C. M. Bender, *Contemp. Phys.* **46**, 277 (2005).
- [77] S. Gopalakrishnan and M. J. Gullans, *Phys. Rev. Lett.* **126**, 170503 (2021).
- [78] C. H. Lee, [arXiv:2011.09505](https://arxiv.org/abs/2011.09505).
- [79] L. Vidmar, L. Hackl, E. Bianchi, and M. Rigol, *Phys. Rev. Lett.* **121**, 220602 (2018).
- [80] L. Vidmar and M. Rigol, *Phys. Rev. Lett.* **119**, 220603 (2017).
- [81] L. Vidmar, L. Hackl, E. Bianchi, and M. Rigol, *Phys. Rev. Lett.* **119**, 020601 (2017).
- [82] L. Hackl, L. Vidmar, M. Rigol, and E. Bianchi, *Phys. Rev. B* **99**, 075123 (2019).
- [83] I. Peschel and V. Eisler, *J. Phys. A: Math. Theor.* **42**, 504003 (2009).
- [84] P. Łydźba, M. Rigol, and L. Vidmar, *Phys. Rev. Lett.* **125**, 180604 (2020).
- [85] P.-Y. Chang, J.-S. You, X. Wen, and S. Ryu, *Phys. Rev. Research* **2**, 033069 (2020).
- [86] R. Modak and T. Nag, *Phys. Rev. Research* **2**, 012074(R) (2020).
- [87] R. Hamazaki, K. Kawabata, and M. Ueda, *Phys. Rev. Lett.* **123**, 090603 (2019).
- [88] Y. N. Joglekar and J. L. Barnett, *Phys. Rev. A* **84**, 024103 (2011).
- [89] A. Mostafazadeh, *Int. J. Geom. Methods Mod. Phys.* **7**, 1191 (2010).